Optimization for multi-cell thin-walled tubes under quasi-static three-point bending

Emre İsa ALBAK (emrealbak@uludag.edu.tr)
Bursa Uludağ University https://orcid.org/0000-0001-9215-0775

Research Article

Keywords: Three-point bending, crashworthiness, COPRAS, multi-objective optimization, multi-cell thin-walled tube

Posted Date: April 8th, 2022

DOI: https://doi.org/10.21203/rs.3.rs-1143441/v1

Version of Record: A version of this preprint was published at Journal of the Brazilian Society of Mechanical Sciences and Engineering on April 25th, 2022. See the published version at https://doi.org/10.1007/s40430-022-03525-8.

Emre İsa ALBAK* (ORCID ID: 0000-0001-9215-0775)

*The Programme of Hybrid and Electric Vehicle Technologies, Bursa Uludağ University, Bursa 16600, Turkey

Corresponding author: Emre İsa ALBAK
The Programme of Hybrid and Electric Vehicle Technologies, Bursa Uludağ University, Bursa 16600, Turkey
emrealbak@uludag.edu.tr

Declarations

Funding
Not applicable

Conflicts of interest/Competing interests
I have no conflicts of interest to disclose.

Availability of data and material
Not applicable

Code availability
Not applicable

Authors' contributions
Emre İsa ALBAK: The article was written by an author.

Optimization for multi-cell thin-walled tubes under quasi-static three-point bending

Abstract

Approaches such as changing the cell number, changing the rib direction, and adding internal structure are utilized to acquire a multi-cell thin-walled structure, and these approaches have meaningful effects on the crashworthiness performance of multi-cell thin-walled tubes. In this study, a comprehensive review is done by using and comparing these approaches together under quasi-static three-point bending conditions. A different crashworthiness indicator is better for each of the produced multi-cell thin-walled structures. The overall best tubes are determined by the complex proportion assessment (COPRAS), a multi-criteria decision-making technique. The weights used in the COPRAS technique are calculated by the entropy method. Thus, two different tubes are chosen as the best ones. Then, multi-objective optimization is performed on these tubes with the multi-objective genetic algorithm (MOGA). The surrogate models of PCF and SEA, which are defined as the objectives in multi-objective optimization studies, are obtained by the (radial basis functions) RBF. Multi-objective optimized multi-cell thin-walled W1L1 and W1L1S1 tubes achieved the same SEA values as the W0L0 square tube at 13.1% and 15.4% lower PCF values, respectively.

Keywords: *Three-point bending, crashworthiness, COPRAS, multi-objective optimization, multi-cell thin-walled tube*

1. Introduction

It is important to absorb the impact energy generated to ensure the safety of the passengers and driver during a traffic accident. The B pillar, side door beam and bumper are important components used to absorb this impact energy. Recently, multi-cell thin-walled tubes have drawn increasing attention because of their great energy absorption characteristic and lightweight [1-3]. Multi-cell thin-walled structures are investigated under various loading conditions such as axial [4-6], oblique [7-9] and lateral [10,11] loading cases.

In recent years, different approaches have been tried by researchers to increase the crashworthiness capacity of multi-cell thin-walled structures [12-15]. Wang et al. [16] studied the performances of the multi-cell thin-walled square tubes, with the cell amounts range from 1 × 1 to 15 × 15 under axial loading cases. Their study indicated that for a multi-cell thin-walled tube, the most critical element in enhancing crashworthiness performance is optimizing the half-wavelength. Wang et al. [17] studied the bending performances of multi-cell square structures under three-point bending. They presented that the number of cells has a meaningful effect on the bending strength of the tube and that high cell number does not always lead to high energy absorption efficiency. Zhang et al. [18] studied bending collapse responses of embedded multi-cell thin-walled tubes under three-point bending. They revealed that the bending capacity of embedded multi-cell thin-walled structures is met to account for about 65–72% of corresponding conventional multi-cell structures.

Multi-cell thin-walled tubes can also be created by joining inner ribs into simple conventional structures and multi-cell tubes or inspired by nature [19-22]. Albak [23] investigated the crashworthiness capacity of multi-cell square thin-walled tubes under axial loading cases by adding square, hexagonal, octagonal and circular structures to the intersections of the walls. The study revealed that the structures added to the wall intersections improve the crashworthiness performance. Hu et al. [24] comprehensively explored energy absorption performances of a bionic honeycomb tubular nested structure inspired by bamboo under axial impact conditions. In their studies, they added circular structures to the wall intersection areas and analysed the effects of the diameter of the circular structure, length of the junction plate and wall thickness of the circular structure parametrically. The study showed that the influence of the diverse mean diameter of the circular structure and length of the junction plate on the energy absorption performances. Du et al. [25] investigated the bending collapse performance and energy absorption characteristics of thin-walled tubes with the mono-box multi-cell cross-section under three-point bending condition. The energy absorption performances of thin-walled tubes with mono-box multi-cell cross-sections are high to thin-walled tubes with mono-box mono-cell sections under the equal mass, and its energy absorption performance will enhance gradually with the number of web regions increased. Huang et al. [26] studied the lateral indentation responses of different multi-cell thin-walled tubes. For thin-walled tubes of equal mass and uniform wall thickness, two-cell and four-cell thin-walled tubes show better energy absorption performance than a mono-cell tube. The specific energy absorption of two-cell and four-cell tubes are 10% and 26% higher, respectively, than that of single-cell at quasi-static loading. Zheng et al. [27] investigated the energy absorption characteristics of fully clamped multi-cell square structures under transverse loading conditions. They investigated the influence of rib direction and rib number on energy absorption characteristics. Their study showed that the multi-cell thin-walled structures with rib parallel to the load direction have higher energy absorption characteristics than that with rib perpendicular to the load direction. They also revealed that the effect of increasing the rib number is different according to the rib direction. Wang et al. [28] studied the collision performance of circular multi-cell thin-walled

tubes inspired by the lotus leaf vein branched structure under three-point bending. Their studies revealed that the number of cells, the ratio of the diameters of the cells, and the wall thicknesses have an effect on the crashworthiness performance.

When the above studies are examined, changing the cell number, changing the rib orientation and adding internal ribs are used to create a multi-cell thin-walled tube, and these approaches have significant effects on crashworthiness performance. In studies in the literature, these approaches are generally examined in separate studies. The innovative aspect of this study is that these approaches are examined comparatively in a single study and their advantages and disadvantages are revealed relative to each other. In the study, new multi-cell thin-walled structures are obtained by changing the rib direction vertically, horizontally and diagonally, creating different cell numbers and adding inner ribs. Three-point bending analyses of fifteen different multi-cell thin-walled tubes created with different approaches are examined and their crashworthiness performances are compared. Then, the best tubes are determined by the complex proportion assessment (COPRAS) method and these tubes are optimized. The weights required for the COPRAS method are found using the entropy approach. Finally, multi-objective optimization is applied with the MOGA for the selected best tubes.

2. Geometrical description and finite element model

2.1. Geometrical description

In this study, the crash performance of fifteen different multi-cell thin-walled structures under quasi-static three-point bending is investigated. The tubes have a square outer wall with a side length of 30 mm. In order to obtain multi-cell structures, different numbers of vertical, horizontal and diagonal walls are added to the square wall. Also, multi-cell tubes are created by adding the square and circular internal structures. The diameter of the circles and the diagonal length of the squares used in the interior are 12.5 mm. While addressing the names of the tubes, if there are vertical, horizontal and diagonal structures, their first letters are used and their numbers are indicated. In addition, the first letters of the square and circular cylindrical internal structures are used. All tubes used in this paper and their nomenclature are given in Fig. 1.

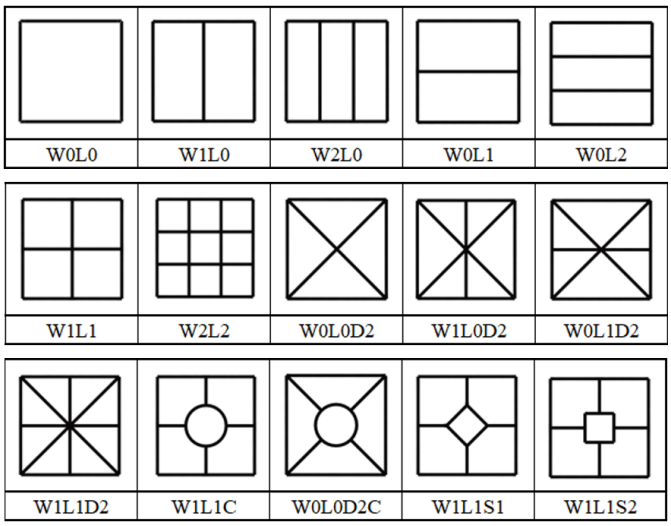

Fig. 1. The cross-sections of multi-cell thin-walled tubes.

In this study, fifteen basic cross-sections that can be obtained by the above-mentioned approaches are examined in order to prevent the increase in the complexity of the multi-cell thin-walled tubes. Similar multi-cell thin-walled structures can also be obtained using different approaches and different geometric cross-sections. Although simpler structures are preferred as energy absorbers, multi-cell thin-walled tubes can be preferred in conditions where more performance is desired. In addition, with the development of advanced production methods such as 3D printers, the production of multi-cell thin-walled tubes will be easier and cheaper.

2.2. Crashworthiness indicators

To measure the crashworthiness performances of the multi-cell thin-walled structures, it is critical to state crashworthiness indicators. The most used crash indicators by researchers are the peak crushing force (PCF), specific energy absorption (SEA), energy absorption (EA), mean crushing force (MCF) and crushing force efficiency (CFE) [29, 30]. PCF is defined as the maximum crushing force during the whole impact process. SEA is the energy absorption of the tube per mass. The SEA is described as:

$$SEA = \frac{EA}{M} \tag{1}$$

where *M* is the overall mass of the tube, and EA is the total energy absorption of the thin-walled tube. The EA can be given as:

$$EA = \int_0^S F(x)dx \tag{2}$$

where *F(x)* is the instantaneous crushing force and *S* is the total crushing displacement of the indenter.

CFE is calculated as the ratio of the mean impact force to the highest impact force:

$$CFE = \frac{MCF}{PCF} \tag{3}$$

where MCF is the average crushing force and can be described as:

$$MCF = \frac{EA}{S} \tag{4}$$

2.3. Simulation model

The researchers have examined the three-point bending test of energy absorbers under dynamic load [28] or quasi-static conditions [31-33]. In order to evaluate the crashing performances of multi-cell thin-walled structures, the finite element (FE) model of the tubes under the quasi-static three-point bending is established using explicit non-linear finite element code RADIOSS [34]. The schematic and finite element model of the multi-cell thin-walled tubes is given in Fig. 2. The finite element model consists of a specimen, an impactor and two supports. As shown in Fig. 2, the specimen is located on two cylindrical supports and crushed by a cylindrical impactor in the center. All components are created using qeph shell formulation four-node element using five through-thickness integration points. Contact definitions are made between specimen and impactor and supports. Also, the contact is

carried out to simulate self-contact of the multi-cell thin-walled tubes to prevent mutual interpenetration. The friction coefficients for all contacts are described as 0.3 [35].

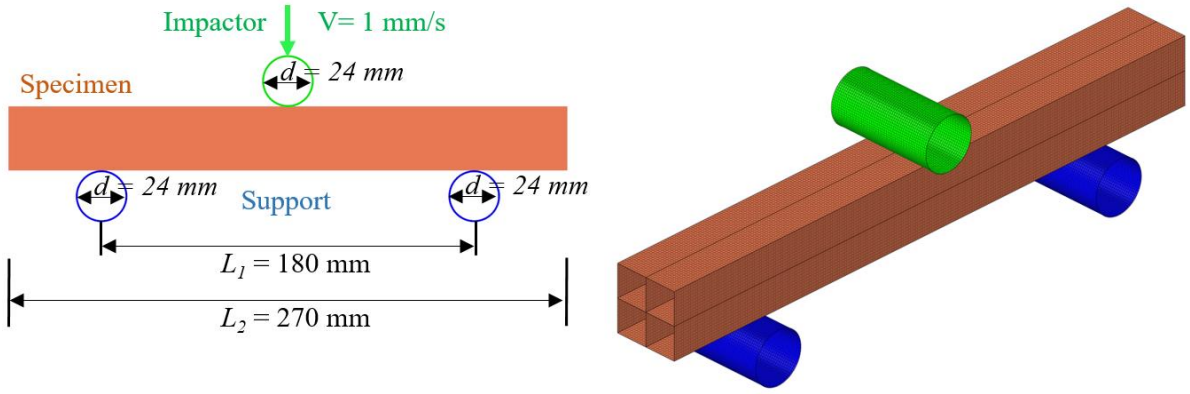

Fig. 2. The schematic and simulation model of the tubes

The mesh convergence analysis is performed as presented in Fig. 3. The analysis is executed on an Intel® Core® i5-8265U CPU running at 1.8 GHz with 8 GB of memory. MCF values less than 1.25 mm are very close to each other. And, computational time increased after 1 mm. So, the average element size is determined as 1 mm, considering accuracy and computational time.

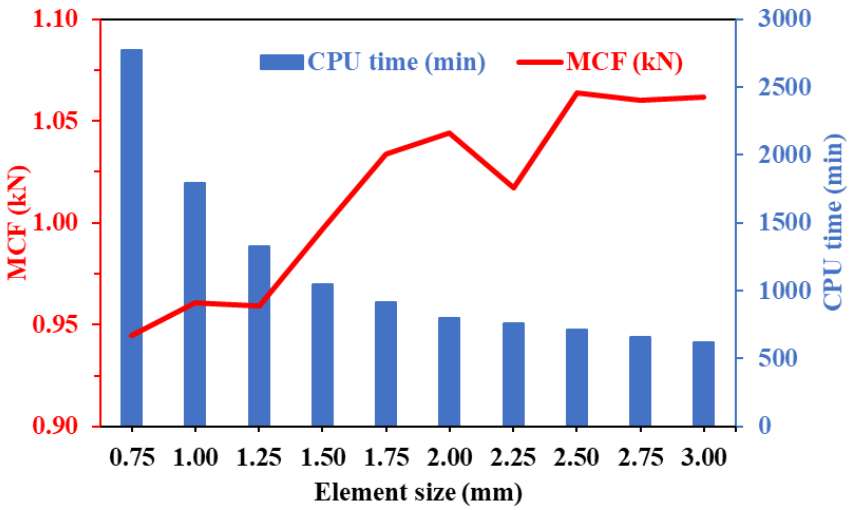

Fig. 3. The mesh convergence analysis of the finite element model

The material AA6063-O is modeled by isotropic elastoplastic material model Mat36 in RADIOSS. Mat36 material definition simulates an isotropic elasto-plastic material with user-defined functions for the work-hardening portion of the stress-strain curve. The mechanical characteristics of AA6063-O are presented in Table 1. The engineering strain-stress curve of AA6063-O is presented in Fig. 4.

Table 1. The mechanical properties of AA6063-O [35]

	Young' modulus (GPa)	Poisson's ratio	Density (g/cm^3)	Yield stress (MPa)	Ultimate stress (MPa)
AA6063-O	68.9	0.33	2.7	28.5	91.4

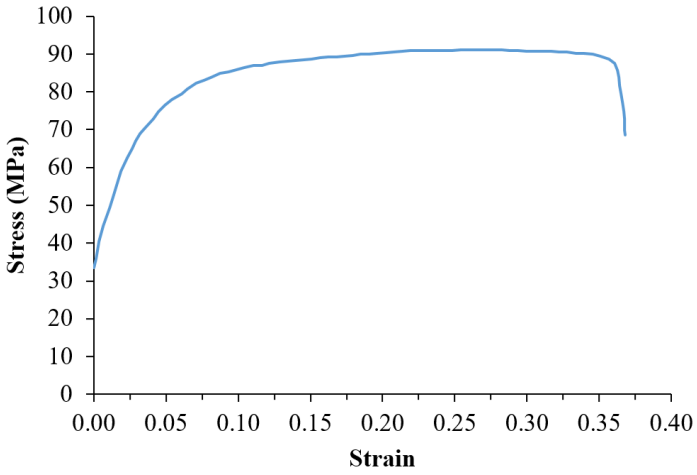

Fig. 4. The engineering stress–strain curve of AA6063-O [35]

2.4. Validation of the simulation model

Literature have been utilized to validate the finite element model to be employed in the paper. Huang and Zhang [35] have conducted quasi-static three-point bending experiments for thin-walled square section tubes. In order to validate the accuracy of the finite element model, the same structural parameters, section properties and experimental requirements as in Ref. [35] are applied. Experimental and finite element analysis deformation modes are given in Fig. 5. The deformation patterns of finite element analysis have good agreement with the experiment. In Fig. 6, force-displacement curves of the experiment and finite element analysis are given. As with the deformation modes of the finite element model, the force-displacement curves have a parallel trend with the experimental test data. The comparison of the initial peak force (IPCF) and MCF values received from the curve of the experimental test and the values obtained as a result of the finite elements is given in Table 2. The maximum relative error for these two indicators is below 4%. Overall, the finite element model developed in this paper has been adequately validated and can be used to explore the crashworthiness characteristics of the multi-cell thin-walled tubes.

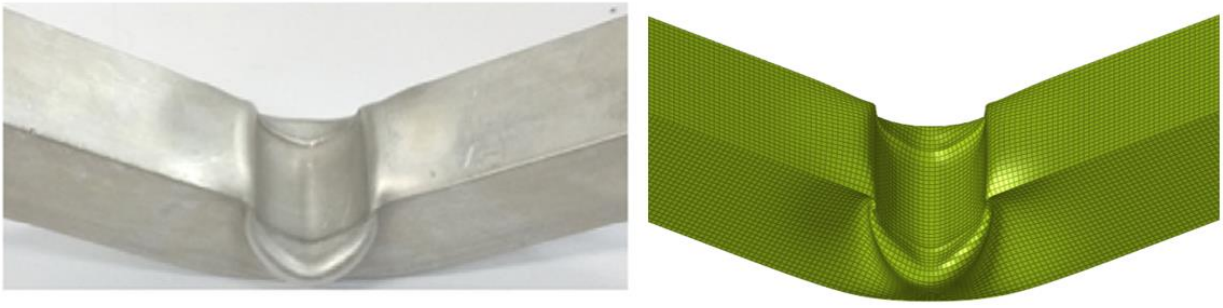

Fig. 5. Experimental [35] and finite element analysis deformation modes

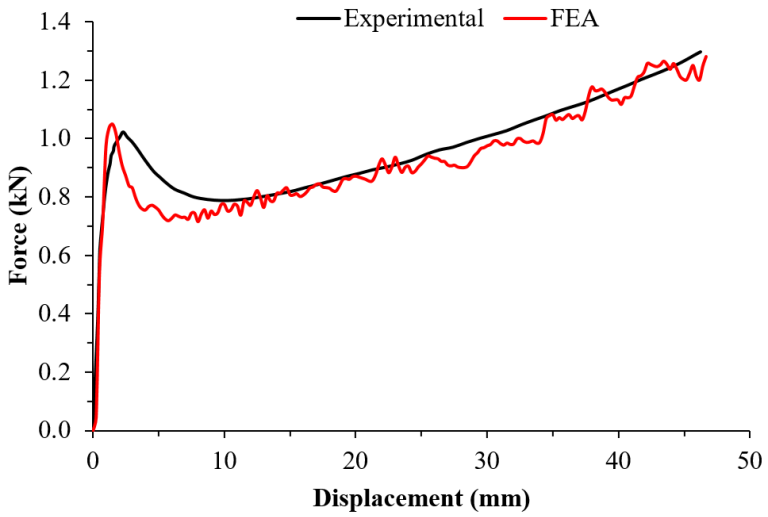

Fig. 6. Force-displacement curves of the experiment [35] and finite element analysis

Table 2. Comparison of the crashworthiness indicators of the experimental [35] and finite element simulation

	Experimental		Finite element		Relative error (%)	
Indicator	IPCF (kN)	MCF (kN)	IPCF (kN)	MCF (kN)	IPCF (kN)	MCF (kN)
Model	1.02	0.92	1.05	0.95	2.94%	3.26%

3. Finite element analysis results

In this section, the crashworthiness performances of the multi-cell thin-walled tubes are discussed. All multi-cell thin-walled tube variants have different wall thicknesses with the same weight. Thus, all comparisons are made with the same weight. The deformation patterns, impact force-displacement curves and crash criteria of multi-cell thin-walled tubes are given in Fig. 7, 8 and 9, respectively.

When the deformation modes of W1L0, W2L0, W1L0D2, W0L1D2 and W1L1D2 tubes are studied, it is seen that local bending collapse occurs. When the force-displacement curves of these multi-cell thin-walled tubes are investigated, it is seen that the force values increase up to a certain point and then decrease. This can also be seen in the crashworthiness criteria. The CFE and SEA of these multi-cell thin-walled tubes are lower than the other tubes. Only the W0L1D2 tube has the highest CFE. The reason for this is that local bending is later than the others. In multi-cell thin-walled tubes other than W1L0, W2L0, W1L0D2, W0L1D2 and W1L1D2, the combination of global bending and local indentation is seen. Crashworthiness performances values for tubes with this deformation mode are generally better than multi-cell thin walled tubes with local bending deformation. The tubes with the highest SEA values are W2L2, W1L1 and W1L1S1 with values of 0.825, 0.805 and 0.763, respectively. The tubes with the highest CFE values are W0L1D2, W1L1S1 and W1L1C with values of 0.907, 0.896 and 0.890, respectively.

When the W1L0 and W2L0 tubes obtained with vertical walls are examined, the PCF values are high, but the CFE and SEA values are low. This shows that only vertical walls do not improve the crashworthiness performance. When W0L1 and W0L2 tubes with only horizontal walls are investigated, it is seen that PCF and CFE values are good, but SEA values are low. In other words, it can be said that horizontal walls partially improve crashworthiness performance. W1L1 and W2L2 tubes, which contain both vertical and horizontal walls, have the highest SEA values and high CFE values, although they have the highest PCF values. This makes these tubes a good energy absorber alternative. Multi-cell thin-walled tubes with diagonal walls have the lowest SEA values. W1L1C, W1L1S1 and W1L1S2 tubes with additional sections added to the intersection points of the walls are the most balanced options in terms of all crashworthiness criteria.

In summary, the best alternatives are W1L1 and W2L2 multi-cell thin-walled tubes with both vertical and horizontal walls, and W1L1C, W1L1S1 and W1L1S2 multi-cell thin-walled structures with additional structures at wall intersections. However, the best multi-cell thin-walled structure cannot be determined directly. It should be determined which of the PCF, CFE and SEA values is more important or at what values to choose for the best multi-cell thin-walled tube. Therefore, in the next sections, selection with the complex proportional assessment (COPRAS) will be explained to determine the best alternatives.

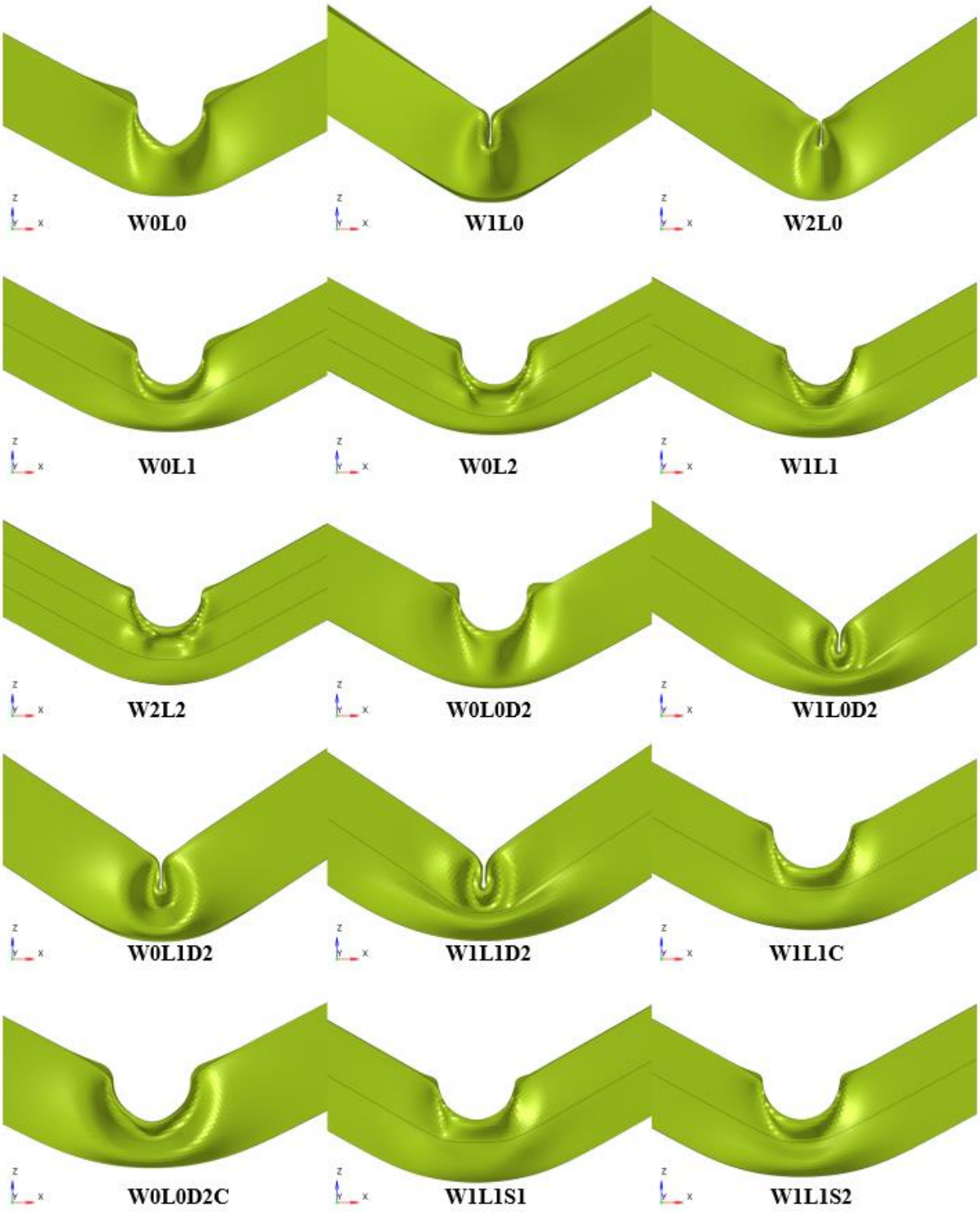

Fig. 7. Deformation modes of the multi-cell thin-walled tubes

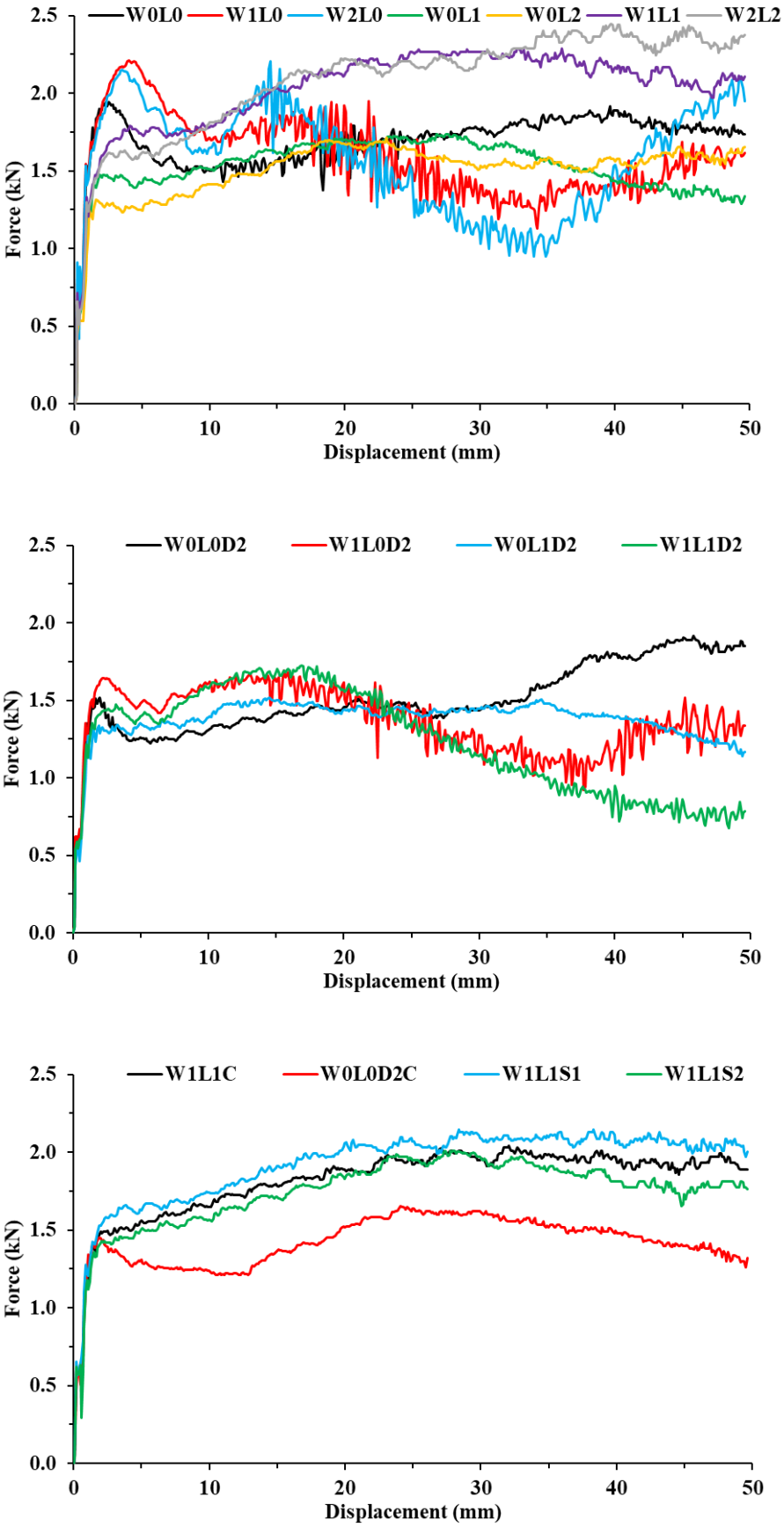

Fig. 8. Force-displacement curves of the multi-cell thin-walled tubes

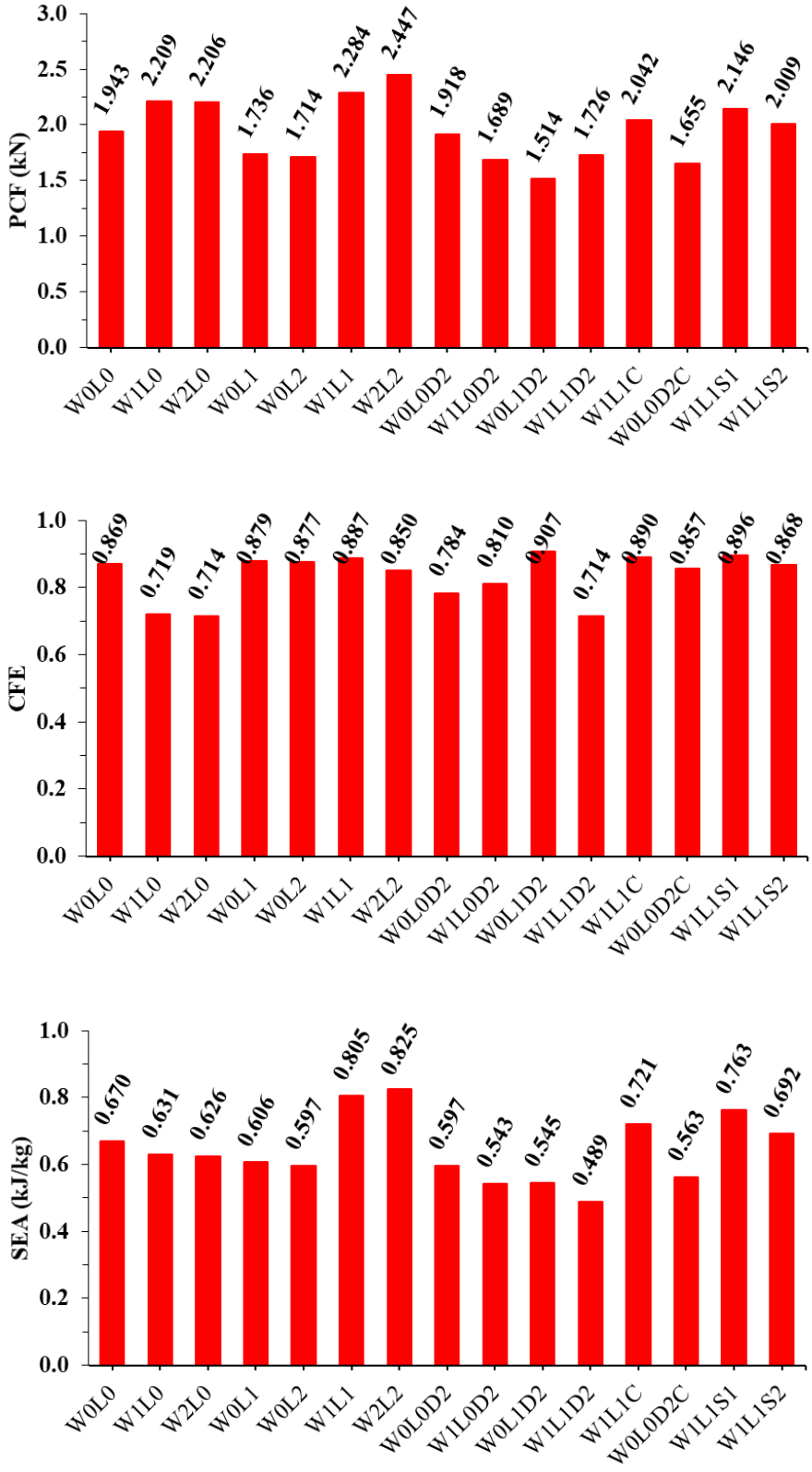

Fig. 9. Crashworthiness criteria of the tubes

4. Selection of the best multi-cell thin-walled tubes

In this study, fifteen different multi-cell thin-walled structures are investigated using three different crashworthiness criteria, PCF, CFE, and SEA. Therefore, it is difficult to choose the best among the considered multi-cell thin-walled structures. So the multi-criteria decision-making study has been utilised for this complex best multi-cell thin-walled structure selection problem. In this work, the complex proportion assessment (COPRAS), which is one of the multi-criteria decision-making approaches, is utilised. COPRAS is commonly used in multi-criteria decision-making cases because of its simplicity [36, 37].

4.1. The complex proportional assessment methodology (COPRAS)

The preference ranking technique of complex proportional assessment (COPRAS) is presented by Zavadskas et al. [38]. The specific steps of the evaluation approach are as follows:

Step 1: Developing the initial decision-making matrix (X):

$$\boldsymbol{X} = [x_{ij}]_{mn} = \begin{bmatrix} x_{11} & x_{12} & & x_{1n} \\ x_{21} & x_{22} & & x_{2n} \\ \cdots & \cdots & \cdots & \cdots \\ x_{m1} & x_{m2} & & x_{mn} \end{bmatrix} \quad (5)$$

where x_{ij} is the quality score of *i*th alternative with respect to *j*th indicator, m is the number of alternatives compared and n is the number of the indicator.

Step 2: Acquiring the normalized decision matrix (R):

$$\boldsymbol{R} = [r_{ij}]_{mn} = \frac{x_{ij}}{\sum_{i=1}^{m} x_{ij}} \quad (6)$$

Step 3: Calculating the weighted normalized decision matrix (D):

$$\boldsymbol{D} = [d_{ij}]_{mn} = r_{ij} \times w_j \quad (7)$$

where d_{ij} is the weighted normalized score of the *i*th alternative with the *j*th indicator.

Step 4: Summing the weighted normalized values for beneficial and non-beneficial attributes:

$$S_{+i} = \sum_{i=1}^{m} d_{+ij} \quad (8)$$

$$S_{-i} = \sum_{i=1}^{m} d_{-ij} \quad (9)$$

where d_{+ij} and d_{-ij} represent normalized weighted values of beneficial and non-beneficial attributes, respectively.

Step 5: Determining the relative importance (Q_i) of each alternative:

$$Q_i = S_{+i} + \frac{\sum_{i=1}^{m} S_{-i}}{S_{-i} \sum_{i=1}^{m} (1/S_{-i})} \quad (10)$$

Step 6: Determining the quantitative utility (U_i) for the *i*th alternative, which presents the rank of the *i*th alternative.

$$U_i = \frac{Q_i}{Q_{max}} \times 100\% \quad (11)$$

Q_{max} is the highest Q_i rate among the Q_i rates. The alternative with the maximum U_i value (100%) is selected as the ideal alternative.

4.2. Entropy method

Weighting is an important element that determines the best alternative for multi-criteria decision-making approaches. Determining the weight depending on subjective preferences may cause the best alternative to be different. Therefore, in this study, the weights are specified by the entropy technique. The entropy technique is frequently used in thin-walled tube selection problems with the ideal crashworthiness characteristics [39, 40]. The entropy technique can be implemented by the following several steps:

Step 1: Developing the initial decision-making matrix (X):

$$\boldsymbol{X} = [x_{ij}]_{mn} = \begin{bmatrix} x_{11} & x_{12} & & x_{1n} \\ x_{21} & x_{22} & & x_{2n} \\ \cdots & \cdots & \cdots & \cdots \\ x_{m1} & x_{m2} & & x_{mn} \end{bmatrix} \quad (12)$$

Step 2: The decision-making matrix should be normalized as p_{ij} with Eq (13):

$$p_{ij} = \frac{x_{ij}}{\sum_{i=1}^{m} x_{ij}}, \ \forall i, j \quad (13)$$

Step 3: Obtain the entropy of the *j*th indicator, E_j:

$$E_j = -(lnm)^{-1} \sum_{i=1}^{m} p_{ij} lnp_{ij}, \ \forall j \quad (14)$$

Step 4: Calculate the distance, d_j:

$$d_j = 1 - E_j \quad (15)$$

Step 5: Indicator weights, w_j, can be given as:

$$w_j = \frac{d_j}{\sum_{i=1}^{n} d_j}, \ \forall j \quad (16)$$

4.3. Finding the best alternatives with COPRAS and entropy

In this section, multi-cell thin-walled tubes will be ranked in terms of their crashworthiness performance with COPRAS and entropy methods. PCF, CFE and SEA indicators are taken into account when ranking the crashworthiness of the tubes. Effective energy absorbers should have high SEA and CFE and low PCF during crashworthiness. Therefore, SEA and CFE are chosen as beneficial indicators and high values are desired, PCF is chosen as the non-beneficial indicator and low value is desired. In the COPRAS method, firstly, the initial decision-making matrix is created with 15 alternative multi-cell thin-walled tubes examined over 3 crashworthiness criteria. The initial decision-making matrix is given in Table 3. The initial decision-making matrix is normalized using Eq.

(7) and presented in Table 4. The weight values of the crashworthiness criteria are calculated by the entropy method and are given in Table 5. After obtaining the weighted normalized matrix, beneficial values and non-beneficial values are obtained. Finally, these values and the relative importance, the quantitative utility and ranking of the alternatives obtained from these values are given in Table 6. The COPRAS method presented the best alternative as W1L1. W1L1S1 is seen as the second-best alternative.

Table 3. The initial decision-making matrix.

Model name	PCF (kN)	CFE	SEA (kJ/kg)
W0L0	1.943	0.869	0.670
W1L0	2.209	0.719	0.631
W2L0	2.206	0.714	0.626
W0L1	1.736	0.879	0.606
W0L2	1.714	0.877	0.597
W1L1	2.284	0.887	0.805
W2L2	2.447	0.850	0.825
W0L0D2	1.918	0.784	0.597
W1L0D2	1.689	0.810	0.543
W0L1D2	1.514	0.907	0.545
W1L1D2	1.726	0.714	0.489
W1L1C	2.042	0.890	0.721
W0L0D2C	1.655	0.857	0.563
W1L1S1	2.146	0.896	0.763
W1L1S2	2.009	0.868	0.692

Table 4. The normalized matrix.

Model name	PCF (kN)	CFE	SEA (kJ/kg)
W0L0	0.0665	0.0694	0.0693
W1L0	0.0756	0.0574	0.0652
W2L0	0.0754	0.0571	0.0647
W0L1	0.0594	0.0702	0.0626
W0L2	0.0586	0.0701	0.0617
W1L1	0.0781	0.0709	0.0832
W2L2	0.0837	0.0679	0.0853
W0L0D2	0.0656	0.0626	0.0617
W1L0D2	0.0578	0.0647	0.0562
W0L1D2	0.0518	0.0725	0.0564
W1L1D2	0.0590	0.0570	0.0506
W1L1C	0.0698	0.0710	0.0745
W0L0D2C	0.0566	0.0684	0.0582
W1L1S1	0.0734	0.0716	0.0789
W1L1S2	0.0687	0.0693	0.0715

Table 5. Weights of crashworthiness indicators obtained by the entropy method.

Crashworthiness indicator	PCF (kN)	CFE	SEA (kJ/kg)
Weights	0.39	0.47	0.14

Table 6. Results of COPRAS.

Model name	S_+	S_-	Q_i	U_i	Rank
W0L0	0.042	0.026	0.0679	0.959	8
W1L0	0.039	0.029	0.0612	0.865	13
W2L0	0.038	0.029	0.0609	0.861	14
W0L1	0.039	0.023	0.0679	0.960	7
W0L2	0.039	0.023	0.0678	0.958	9
W1L1	*0.049*	*0.030*	*0.0708*	*1.000*	*1*
W2L2	0.050	0.033	0.0699	0.988	3
W0L0D2	0.038	0.026	0.0637	0.900	12
W1L0D2	0.036	0.023	0.0649	0.917	11
W0L1D2	0.037	0.020	0.0695	0.982	4
W1L1D2	0.032	0.023	0.0606	0.855	15
W1L1C	0.045	0.027	0.0694	0.980	5
W0L0D2C	0.037	0.022	0.0670	0.946	10
W1L1S1	0.047	0.029	0.0703	0.993	2
W1L1S2	0.043	0.027	0.0681	0.962	6

5. Crashworthiness optimization

In this section, the multi-objective optimization of W1L1 and W1L1S1 tubes, which are determined as the best multi-cell thin-walled tubes by the COPRAS method, will be explained. W1L1 tube is chosen as the best tube in the COPRAS method, while the W1L1S1 is chosen because it is the best tube with an inner structure.

5.1. Description of the optimization problem

It is generally expected that energy absorbers can absorb as much impact energy as possible per unit mass and have a smaller peak crushing force when it is used as a vehicle safety component [28]. For this reason, in this study, multi-objective optimization is carried out with the PCF and SEA indicators as the objectives. Therefore, the optimization case for W1L1 can be expressed as follows:

$$\begin{cases} Min\ \{PCF(t_1,t_2,t_3), -SEA(t_1,t_2,t_3)\} \\ \quad s.t. \begin{cases} 0.5\ mm \le t_1 \le 2.0\ mm \\ 0.5\ mm \le t_2 \le 2.0\ mm \\ 0.5\ mm \le t_3 \le 2.0\ mm \end{cases} \end{cases} \tag{17}$$

where three design variables, namely the outer wall thickness t_1, vertical wall thickness t_2 and lateral wall thickness t_3, which range from 0.5 mm to 2.0 mm, are considered. The optimization problem for W1L1S1 can be formulated as follows:

$$\begin{cases} Min\ \{PCF(t_1,t_2,t_3,t_4), -SEA(t_1,t_2,t_3,t_4)\} \\ \quad s.t. \begin{cases} 0.5\ mm \le t_1 \le 2.0\ mm \\ 0.5\ mm \le t_2 \le 2.0\ mm \\ 0.5\ mm \le t_3 \le 2.0\ mm \\ 0.5\ mm \le t_4 \le 2.0\ mm \end{cases} \end{cases} \tag{18}$$

where four design variables, namely the outer wall thickness t_1, vertical wall thickness t_2, lateral wall thickness t_3 and inner structure wall thickness t_4 which range from 0.5 mm to 2.0 mm, are considered. The design variables of W1L1 and W1L1S1 are given in Fig. 10.

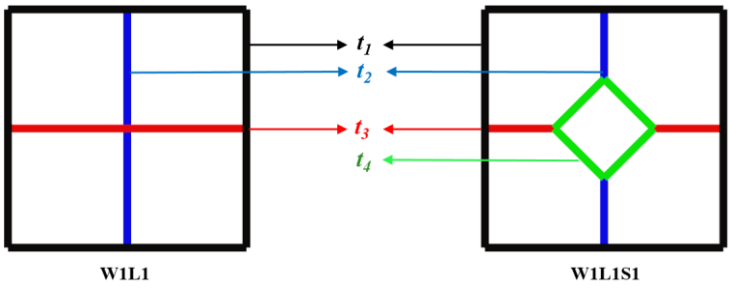

Fig. 10. Design variables of W1L1 and W1L1S1

5.2. Surrogate model

After establishing the optimization case, it is very critical to create the functional relationship between optimization objectives and design variables. It is hard to derive analytically objective functions for PCF and SEA. Because they involve highly non-linear contact-impact and large deformation mechanics. For this reason, surrogate modeling is generally preferred to obtain objective functions in crashworthiness cases [41, 42]. Compared to the other approaches, the (radial basis functions) RBF technique has ensured higher accuracy in crashworthiness optimization cases [43]. Therefore, in this study, the RBF method is chosen to obtain surrogate models of objective functions. The first step of the surrogate modeling is to generate the design area using (design of experiment) DOE techniques. In this study, 30 sample points for W1L1 and 40 sample points for W1L1S1 are created using the Latin hypercube method.

The accuracy of the optimization results depends on the accuracy of the created surrogate models. Therefore, the created surrogate models need to be validated. To measure the accuracy of the created surrogate models, five checking designs are created using the Latin hypercube approach. The relative error (RE) between the response value ($f_{RBF}(x)$) and the finite element simulation ($f_{fea}(x)$) can be expressed as:

$$RE = \left| \frac{f_{fea}(x) - f_{RBF}(x)}{f_{fea}(x)} \right| \tag{19}$$

The RE values of the RBF models for W1L1 and W1L1S1 are presented in Fig. 11. All RE values are less than 7%, indicating that the generated surrogate models have acceptable accuracy and can therefore be applied to multi-objective crashworthiness optimization.

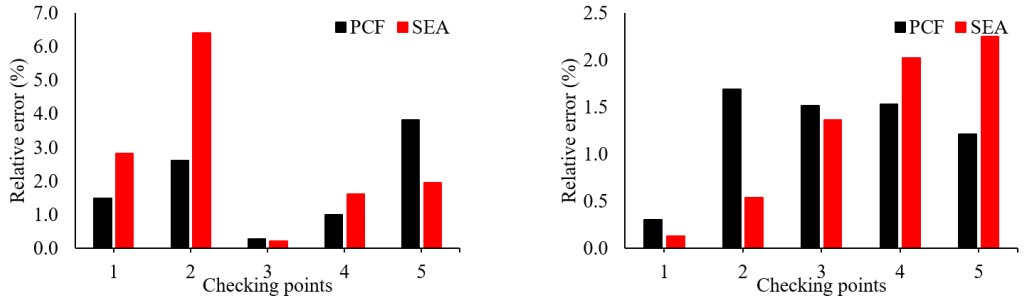

(a) W1L1 (b) W1L1S1

Fig. 11. REs of the surrogate models

5.3. Multi-objective optimization results

In this study, the multi-objective genetic algorithm (MOGA) is used to seek the optimal solutions for W1L1 and W1L1S1. MOGA is one of the multi-objective optimization methods preferred in crashworthiness problems [44, 45]. Fig. 12. presents the Pareto frontiers obtained by the MOGA algorithm. As shown in Fig. 12, the Pareto frontiers are declared by two conflicting crashworthiness criteria PCF and SEA. That is, as one increases, the other decreases and vice versa. Truly, any design in the Pareto front could be ideal. Which design should be chosen is fully determined by the engineering design case. As an example, the force value (1.943 kN) of the W0L0 tube, which consists of only the outer wall, is considered and is indicated by the green line in Fig. 12. In the Pareto frontiers obtained for W1L1 and W1L1S1, the designs corresponding to this force value are considered. Finite element analyzes of the optimum models obtained at these design points are performed and their accuracy is examined. In Table 7, the values obtained as a result of the optimizations, the results of the finite element analysis and the relative errors are given. According to the results, it can be said that the optimizations have sufficient accuracy. The W0L0 model has a PCF of 1.943 kN versus a SEA of 0.67 kJ/kg. In the optimum W1L1 and W1L1S1 designs, 0.773 kJ/kg and 0.758 kJ/kg SEA values are obtained, respectively, at PCF values close to W0L0. As a result, with the optimization study, 13.1% and 15.4% better SEA values were obtained for W1L1 and W1L1S1, respectively, at the same PCF values as the W0L0 model.

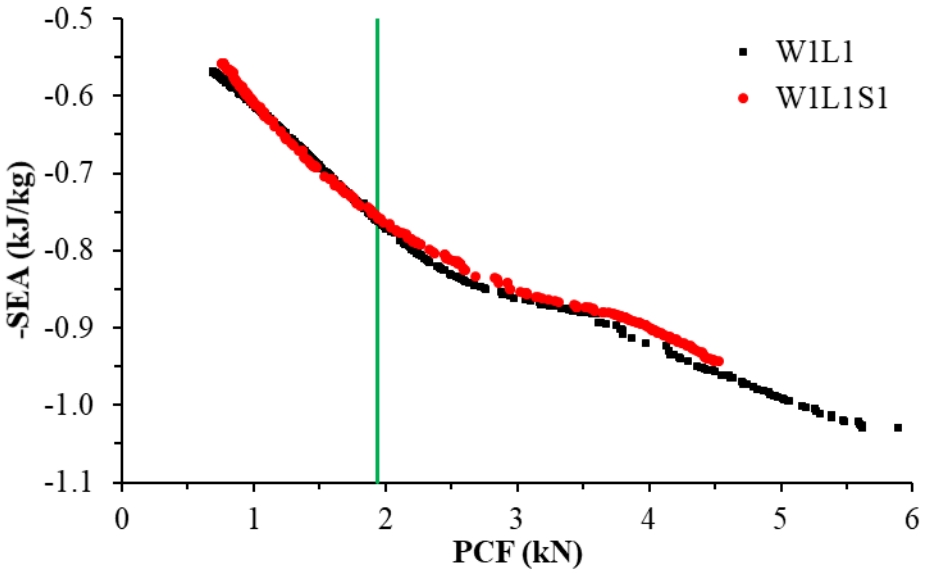

Fig. 12. Pareto frontiers of W1L1 and W1L1S1

Table 7. Optimum points

	Optimization		Finite element analysis		Relative error (%)	
	PCF (kN)	SEA (kJ/kg)	PCF (kN)	SEA (kJ/kg)	PCF (kN)	SEA (kJ/kg)
W0L0	-	-	1.943	0.670	-	-
W1L1	1.951	0.763	2.048	0.773	4.97	1.31
W1L1S1	1.978	0.763	2.008	0.758	1.49	0.66

6. Conclusions

In this study, the crashworthiness performances of fifteen different multi-cell thin-walled tubes under three-point bending are extensively investigated by finite element analysis. The finite element model has been validated with literature test data. The crashworthiness performance of each tube is different, so the best alternatives are determined by the COPRAS method. Since weighting is an important factor in the COPRAS method, the weighting is calculated with the entropy method. W1L1 and W1L1S1 tubes, which are determined as the best alternatives, are optimized with the MOGA method. The surrogate models of PCF and SEA, which are selected as the objectives in multi-objective optimization studies, are obtained by the RBF method. Finally, the optimum designs corresponding to the force value of the W0L0 tube are chosen from the Pareto frontiers to compare the results of the optimizations. Within its limitation of the study, the major conclusions are summarized as follows:

- W1L0 and W2L0 tubes obtained with vertical walls have high PCF values but low CFE and SEA values. This shows that not only vertical walls improve crashworthiness performance.
- W0L1 and W0L2 tubes with only horizontal walls have good PCF and CFE values but low SEA values. In other words, it can be said that the horizontal walls partially improve the crashworthiness performance.
- W1L1 and W2L2 tubes with both vertical and horizontal walls have the highest SEA values and high CFE values despite having the highest PCF values. This makes these tubes a good alternative to energy absorbers.
- W1L1C, W1L1S1 and W1L1S2 tubes with additional sections added to the intersection points of the walls are the most balanced options in terms of all crashworthiness indicators.
- With the optimization study, 13.1% and 15.4% better SEA values were obtained for W1L1 and W1L1S1, respectively, at the same PCF values as the W0L0 model.
- Obtaining multi-cell thin-walled tubes in different shapes in three-point bending conditions is a useful approach to improve crashworthiness performance.

References

[1] Abada M, Ibrahim A (2020) Hybrid multi-cell thin-walled tubes for energy absorption applications: Blast shielding and crashworthiness. Composites Part B: Engineering 183:107720.

[2] Zahran MS, Xue P, Esa MS (2017) Novel approach for design of 3D-multi-cell thin-walled circular tube to improve the energy absorption characteristics under axial impact loading. International Journal of Crashworthiness 22(3):294-306.

[3] Albak Eİ (2021) Crashworthiness design and optimization of nested structures with a circumferentially corrugated circular outer wall and inner ribs. Thin-Walled Structures 167:108219.

[4] Nia AA, Parsapour M (2013) An investigation on the energy absorption characteristics of multi-cell square tubes. Thin-Walled Structures 68:26-34.

[5] Pang T, Zheng G, Fang J, Ruan D, Sun G (2019) Energy absorption mechanism of axially-varying thickness (AVT) multicell thin-walled structures under out-of-plane loading. Engineering Structures 196:109130.

[6] Xie S, Yang W, Li H, Wang N (2017) Impact characteristics and crashworthiness of multi-cell, square, thin-walled, structures under axial loads. International journal of crashworthiness 22(5):503-517.

[7] Fang J, Gao Y, Sun G, Qiu N, Li Q (2015) On design of multi-cell tubes under axial and oblique impact loads. Thin-Walled Structures 95:115-126.

[8] Albak Eİ (2021) Crashworthiness design for multi-cell circumferentially corrugated thin-walled tubes with sub-sections under multiple loading conditions. Thin-Walled Structures 164:107886.

[9] Rad MA, Khalkhali A (2018) Crashworthiness multi-objective optimization of the thin-walled tubes under probabilistic 3D oblique load. Materials & Design 156:538-557.

[10] Bai J, Meng G, Wu H, Zuo W (2019) Bending collapse of dual rectangle thin-walled tubes for conceptual design. Thin-Walled Structures 135:185-195.

[11] Zeng D, Duddeck F (2017) Improved hybrid cellular automata for crashworthiness optimization of thin-walled structures. Structural and Multidisciplinary Optimization 56(1):101-115.

[12] Tran T (2017) Crushing and theoretical analysis of multi-cell thin-walled triangular tubes under lateral loading. Thin-Walled Structures 115:205-214.

[13] Albak Eİ (2021) Multi-objective crashworthiness optimization of thin-walled multi-cell tubes with different wall lengths. International Journal of Crashworthiness 26(4):438-455.

[14] Attar AA, Rasouli SA, Chahardoli S (2020) Effect of combined multi-cell columns and exterior stiffeners on energy absorption parameters of thin-walled tubes under axial load. Journal of the Brazilian Society of Mechanical Sciences and Engineering 42(9):1-16.

[15] Li Z, Ma W, Yao S, Xu P (2021) Crashworthiness performance of corrugation-reinforced multicell tubular structures. International Journal of Mechanical Sciences 190:106038.

[16] Wang Z, Liu J, Yao S (2018) On folding mechanics of multi-cell thin-walled square tubes. Composites Part B: Engineering 132:17-27.

[17] Wang Z, Li Z, Zhang X (2016) Bending resistance of thin-walled multi-cell square tubes. Thin-Walled Structures 107:287-299.

[18] Zhang X, Zhang H, Leng K (2018) Experimental and numerical investigation on bending collapse of embedded multi-cell tubes. Thin-Walled Structures 127:728-740.

[19] Albak Eİ, Solmaz E, Yıldız AR, Öztürk F (2021) Multiobjective crashworthiness optimization of graphene type multi-cell tubes under various loading conditions. Journal of the Brazilian Society of Mechanical Sciences and Engineering 43(5):1-19.

[20] Zhang Y, Wang J, Wang C, Zeng Y, Chen T (2018) Crashworthiness of bionic fractal hierarchical structures. Materials & Design 158:147-159.

[21] Huang H, Xu S (2019) Crashworthiness analysis and bionic design of multi-cell tubes under axial and oblique impact loads. Thin-Walled Structures 144:106333.

[22] Zhang L, Bai Z, Bai F (2018) Crashworthiness design for bio-inspired multi-cell tubes with quadrilateral, hexagonal and octagonal sections. Thin-Walled Structures 122:42-51.

[23] Albak Eİ (2020) Effects of sections added to multi-cell square tubes on crash performance. Materials Testing 62(5):471-480.

[24] Hu D, Wang Y, Song B, Dang L, Zhang Z (2019) Energy-absorption characteristics of a bionic honeycomb tubular nested structure inspired by bamboo under axial crushing. Composites Part B: Engineering 162:21-32.

[25] Du Z, Duan L, Cheng A, Xu Z, Zhang G (2019) Theoretical prediction and crashworthiness optimization of thin-walled structures with single-box multi-cell section under three-point bending loading. International Journal of Mechanical Sciences 157:703-714.

[26] Huang Z, Zhang X, Zhang H (2018) Energy absorption and optimization design of multi-cell tubes subjected to lateral indentation. Thin-Walled Structures 131:179-191.

[27] Zheng D, Zhang J, Lu B, Zhang T (2021) Energy absorption of fully clamped multi-cell square tubes under transverse loading. Thin-Walled Structures 169:108334.

[28] Wang Y, He Q, Shi X, Zhong J (2021) Crashworthiness analysis and multi-objective optimisation of a novel circular tube under three-point bending. International Journal of Crashworthiness 1-14. Doi:10.1080/13588265.2021.1926860.

[29] Li S, Guo X, Li Q, Sun G (2020) On lateral crashworthiness of aluminum/composite hybrid structures. Composite Structures 245:112334.

[30] Demirci E, Yıldız AR (2018) An experimental and numerical investigation of the effects of geometry and spot welds on the crashworthiness of vehicle thin-walled structures. Materials Testing 60(6):553-561.

[31] Eyvazian A, Moeinifard M, Musharavati F, Taghizadeh SA, Mahdi E, Hamouda AM, Tran TN (2021) Mechanical behavior of resin pin-reinforced composite sandwich panels under quasi-static indentation and three-point bending loading conditions. Journal of Sandwich Structures & Materials 23(6):2127-2145.

[32] Asaee Z, Montesano J, Worswick M (2021) Assessing the failure mechanisms and mechanical performance of Co-moulded hybrid AA5182-O/GFRP hat-channel beams under quasi-static three-point bending. Composite Structures 256:113007.

[33] Farrokhabadi A, Taghizadeh SA, Madadi H, Norouzi H, Ataei A (2020) Experimental and numerical analysis of novel multi-layer sandwich panels under three point bending load. Composite Structures 250:112631.

[34] Radioss (2019) Radioss Manual. Altair Engineering, Inc

[35] Huang Z, Zhang X (2018) Three-point bending collapse of thin-walled rectangular beams. International Journal of Mechanical Sciences 144:461-479.

[36] Zheng G, Wu S, Sun G, Li G, Li Q (2014) Crushing analysis of foam-flled single and bitubal polygonal thin-walled tubes. Int J Mech Sci 87:226–240

[37] Zou X, Gao G, Dong H, Xie S, Chen G, Tan T (2017) Crashworthiness analysis and structural optimisation of multi-cell square tubes under axial and oblique loads. Int J Crashworthiness 22(2):129–147

[38] Zavadskas EK, Turskis Z, Tamošaitiené J, Marina V (2008) Multicriteria selection of project managers by applying grey criteria. Technol Econ Dev Econ 14(4):462–477

[39] Xiong F, Wang D, Ma Z, Lv T, Ji L (2019) Lightweight optimization of the front end structure of an automobile body using entropy-based grey relational analysis. Proceedings of the Institution of Mechanical Engineers, Part D: Journal of Automobile Engineering 233(4):917-934.

[40] Xu, X., Zhang, Y., Chen, X., Liu, Z., Xu, Y., & Gao, Y. (2019). Crushing behaviors of hierarchical sandwich-walled columns. International Journal of Mechanical Sciences, 161, 105021.

[41] Sun G, Pang T, Fang J, Li G, Li Q (2017) Parameterization of criss-cross configurations for multiobjective crashworthiness optimization. International Journal of Mechanical Sciences 124:145-157.

[42] Pirmohammad S, Esmaeili-Marzdashti S (2019) Multi-objective crashworthiness optimization of square and octagonal bitubal structures including different hole shapes. Thin-Walled Structures 139:126-138.

[43] Fang H, Rais-Rohani M, Liu Z, Horstemeyer MF (2005) A comparative study of metamodeling methods for multiobjective crashworthiness optimization. Computers & structures 83(25-26):2121-2136.

[44] Yao S, Huo Y, Yan K, Xu P (2019) Crashworthiness study on circular hybrid corrugated tubes under axial impacts. Thin-Walled Structures 145:106358.

[45] Paz J, Díaz J, Romera L, Costas M (2014) Crushing analysis and multi-objective crashworthiness optimization of GFRP honeycomb-filled energy absorption devices. Finite Elements in Analysis and Design 91:30-39.